Journal of Elasticity **61:** 49–81, 2000.

Structure, Mechanical Properties, and Mechanics of Intracranial Saccular Aneurysms

J.D. HUMPHREY[1] and P.B. CANHAM[2]
[1]*Biomedical Engineering, Texas A&M University, College Station, TX, U.S.A.*
E-mail: jdh@acs.tamu.edu
[2]*Medical Biophysics, University of Western Ontario, London, Ontario, Canada*

Received 20 April 2000; in revised form 13 February 2001

Abstract. Intracranial saccular aneurysms remain an enigma; it is not known why they form, why they enlarge, or why only some of them rupture. Nonetheless, there is general agreement that mechanics plays an essential role in each aspect of the natural history of these potentially deadly lesions. In this paper, we review recent findings that discount limit point instabilities under quasi-static increases in pressure and resonance under dynamic loading as possible mechanisms of enlargement of saccular aneurysms. Indeed, recent histopathological data suggest that aneurysms enlarge due to a stress-mediated process of growth and remodeling of collagen, the primary load-bearing constituent within the wall. We submit that advanced theoretical, experimental, and numerical studies of this process are essential to further progress in treating this class of pathologies. The purpose of this review is to provide background and direction that encourages elasticians to contribute to this important area of research.

Key words: collagen structure, stability, rupture criterion, growth mechanics.

1. Introduction

Intracranial aneurysms are focal dilatations of the arterial wall that usually occur in or near the circle of Willis, the primary network of vessels that supplies blood to the brain. In general, these aneurysms occur in one of two forms: *fusiform lesions*, which are elongated dilatations of an artery, and *saccular lesions*, which are local sac-like out-pouchings. This paper focuses on the more common saccular form, which usually develops at the apex of a bifurcation (Figure 1). Rupture of saccular aneurysms is the leading cause of spontaneous subarachnoid hemorrhage (*SAH*), which despite advances in neurosurgery and neuroradiology continues to result in a high mortality rate (35–50%) and severe morbidity among the survivors [20, 26, 102]. Fortunately, with advances in medical imaging, greater numbers of unruptured aneurysms are being detected. There are two primary methods of treating these lesions: intracranial surgery, wherein the lesion is isolated from the blood flow by placing a small metal clip at its neck, and catheter-based interventions, which include the deployment of metallic coils that promote the formation of clots within the lesion that again isolate it from the blood flow [10, 71]. Conservative

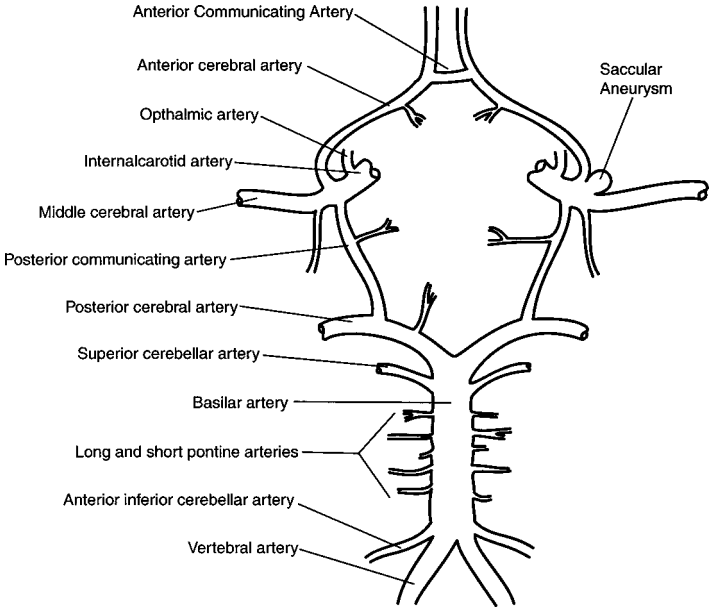

Figure 1. Schema of the cerebral vasculature illustrating the circle of Willis and surrounding arteries; shown, too, is a typical aneurysm at a bifurcation (where the fundus = pole).

management is also a clinical option, however, for it is thought that many saccular aneurysms will not rupture [10, 26, 80]. For example, a recent international trial [103] reported a small risk of rupture ($\sim$0.1% per year) for aneurysms less than 10 mm in maximum dimension; these results have generated considerable controversy, however (e.g., [4]). The primary clinical dilemma, therefore, is whether a patient should be subjected to a prophylactic procedure that has associated risks given that it is unlikely that the aneurysm will rupture, or if it is better to monitor periodically the patient for changes in the lesion while accepting the devastating consequences associated with *SAH* should a rupture occur.

The goals of this paper are threefold: to review our current knowledge of the biology and structure of saccular aneurysms, to assess recent developments that address the associated mechanics, and to identify questions about aneurysmal development, enlargement, and rupture that require further biomechanical study. One goal of histo-mechanical analysis, for example, is to predict better the likelihood of enlargement of a given lesion and its rupture-potential, the former of which may occur over periods from weeks to decades. It is hoped, therefore, that this paper stimulates experimental, theoretical, and computational research that will complement that in the basic and clinical sciences and thereby contribute to improved treatment strategies.

2. Natural History and Significance

Two-to-five percent of the general population in the Western World likely harbors a saccular aneurysm, ruptured or unruptured. Histopathological and clinical studies reveal further that these lesions are more prevalent in women (55–65%), and that they occur predominantly in the anterior and middle portions of the cerebral vasculature (cf. Figure 1). For example, a review by Ferguson [26] reports distributions of 37% in the internal carotid artery, 31% in the anterior cerebral and anterior communicating arteries, 13% in the middle cerebral artery, 9% in the basilar artery, 5% in the vertebral artery, and 5% other; different reports indicate a slightly higher percentage in the middle cerebral artery, but are otherwise similar [92, 98]. Multiple lesions occur in ∼15–30% of aneurysm patients. Although saccular aneurysms may remain dormant for years to decades, the small percentage that rupture tend to do so during the 5th–7th decades of life (mean age ∼52 years old). For more detail, see Sekhar and Heros [80], Hashimoto and Handa [38], Kassel and Torner [52], and Wiebers et al. [102].

The natural history of saccular aneurysms consists of at least three phases: pathogenesis, enlargement, and rupture. The initiation of saccular aneurysms is the subject of considerable debate, but it is generally accepted that unique structural features of the cerebral vasculature contribute to the pathogenesis (e.g., [7, 80]). Cerebral arteries do not have an external elastic lamina, they have sparse medial elastin, they lack supporting perivascular tissue, and they have structural irregularities at the apex of their bifurcations [27, 40, 91]. It is thought that these factors may render the cerebral artery susceptible to a local weakening of the wall under the persistent action of hemodynamic loads, particularly in hypertension [92]. One theme, in particular, is that the internal elastic lamina and muscular media must become markedly fragmented or degraded in order for a saccular aneurysm to form [11, 24, 80]. Other risk factors may include heavy alcohol consumption, cigarette smoking, and the long term use of analgesics or oral contraceptives, although these are thought to play a lesser role (see [20, 73, 103]). Increased familial incidence in some populations suggests that genetics is important. It has been hypothesized, for example, that a genetic defect may disrupt the normal synthesis of certain types of collagen (e.g., types III and V) within the cerebral vasculature, which in turn may weaken the arterial wall [41, 74]. Similarly, it has been hypothesized that an asymmetrically formed circle of Willis may be of genetic origin, and may increase the hemodynamic load on portions of the vasculature [20, 92]. There is a pressing need for much more research on the roles of genetics, risk factors, cellular responses to mechanical stresses, and hemodynamics in the pathogenesis.

Aneurysms typically enlarge from the initially small out-pouching or dilatation of the arterial wall, which can result in lesions having diameters up to 30 mm as well as complex shapes and composition. Unfortunately, little is known about the mechanisms by which this enlargement occurs, or its time-course. Some recent studies suggest that slower rates of enlargement are associated with a lower risk of

rupture [51, 66]. Regardless, among other hypotheses, it has been suggested that lesions may enlarge rapidly due to structural instabilities, that is via either a limit point instability or resonance. These two hypotheses are discussed below based on more recent nonlinear analyses and shown unlikely, at least for particular classes of lesions. As it will be seen, there is a pressing need for an increased understanding of this critical phase of the natural history.

Rupture of an aneurysm implies one of two outcomes: a catastrophic tearing of a portion of the lesion, with significant bleeding that is often fatal, or a small "leak", with minimal bleeding but clinical symptoms. Small leaks may be sealed by a fibrin patch and followed by the formation of an intraluminal or intramural thrombus; such repair may render the lesion more susceptible to subsequent enlargement or catastrophic rupture. Although histomechanical failure mechanisms are unknown, rupture usually occurs at the fundus (Figure 1) despite the neck often being thinner [18, 80]. Moreover, in the case of coexisting aneurysms, the larger one usually ruptures first, or if of nearly the same size, the proximal one will usually rupture first [18, 50].

Several studies have associated various physical factors with rupture-potential. Asari and Ohmoto [3] suggested that it is the combination of lesion location (e.g., middle cerebral artery), shape (i.e., multilobular or not), and the presence of hypertension that best indicates a high risk of rupture. Hademenos et al. [35] similarly reported that multilobular lesions are more prone to rupture, but they suggested further that the less prevalent posterior lesions have a higher chance to rupture. The vast majority of other studies draw conclusions based primarily on the size of the lesion, however, with estimates of the critical maximum dimension ranging from 3 to 10 mm [18, 52, 98, 102, 103]. From a mechanical perspective, of course, shape and wall thickness are more important contributors to rupture-potential than overall size [84]. Ujiie et al. [99] reported that 59% of lesions are round, 24% oval, and 22% barlike; Parlea et al. [75] reported that aneurysms of the anterior communicating artery (recall Figure 1) tended to be pear-shaped, and, although a clear pattern could not be established, most aneurysms tend toward a spherical shape. That shape has not been considered more is particularly surprising since Crompton [17] showed long ago that lesions in women tend to have a greater neck : height ratio and they are more likely to rupture. Lesion thickness can range from 30 to 500 μm in the unloaded configuration [96]. It is believed that increasing thickness corresponds primarily, but not exclusively, with continued enlargement [93]. Based on a study of 23 unruptured lesions, Suzuki and Ohara [96] suggested further that saccular aneurysms fall into one of four categories: uniformly thin (22%), thick at the fundus but thin at the neck (17%), thin at the neck but variable elsewhere (43%), or thick at the neck but variable elsewhere (18%). Asari and Ohmoto [3] report similar findings, including that the uniformly thin lesions tended to be the smallest (less than 4 mm in diameter). Whereas most previous mathematical models have assumed idealized shapes and uniform wall thickness

(in the undeformed configuration), there is a clear need for more complete data upon which more realistic models can be based.

3. Histopathology

Early studies using light microscopy showed relatively little structural organization within saccular aneurysms as compared to the nearby parent arteries [28, 39, 79, 89]. Like other muscular arteries, cerebral arteries consist of three main layers: the tunica adventitia (outer layer) consists primarily of collagen, the tunica media consists primarily of smooth muscle with interspersed collagen and some elastin, and the tunica intima (inner layer) consists primarily of a basement membrane bordered on the luminal side by a single layer of endothelial cells. The transition from parent vessel to aneurysm is characterized by a sharp break in the media [7, 39, 80], thus it is generally thought that the aneurysm stems from the adventitia and intima [69, 79]. Stehbens [89] suggested, however, that the appearance of the aneurysmal wall does not indicate that part of the arterial wall from which the sac came for many of its features seem to be acquired during the later stages of enlargement. Regardless, a general finding is that the aneurysmal wall consists primarily of collagen, with small patches of smooth muscle of the stellate form, as is usually found in the intima of vessels. The elastic lamina also tends to split into several laminae at the neck of the aneurysm and to be fragmented or absent in the aneurysm wall [39, 89]. Stehbens [90] reported that in those portions of an aneurysm that resemble an intimal proliferation, the collagen fibers are sparse, of variable length and caliber, and arranged haphazardly, whereas when the wall is fibrotic, the collagen is arranged in distinct laminae. That the fundus is generally thicker than the neck [80, 89], and yet the site at which rupture is most likely to occur [18, 79, 92], is one of the unresolved paradoxes of aneurysm structure.

Electron microscopy has confirmed this general histology, with additional detail regarding the presence of monocytes, fibroblasts, macrophages, and cellular debris [60, 72, 92]. Spatial variations in these cell types provide possible clues with regard to lesion heterogeneity, including local weakening of the wall, and dynamic changes therein [53, 54]. Recent immunocytochemical and immunofluorescence studies reveal further detail on aneurysm composition. Austin et al. [7] found type I collagen and fibronectin to be distributed uniformly throughout the aneurysmal wall, and Mimata et al. [69] identified the fibrillar types I and III collagens, which are mainly responsible for the tensile strength, throughout the wall. The microfibrillar type VI collagen is also distributed throughout the wall, albeit mostly in the outer region, and the basement membrane type IV collagen is localized around the sparsely distributed smooth muscle cells. Kosierkiewicz et al. [55] examined lesions with atherosclerotic involvement. They identified an intimal type thickening even in some small aneurysms and advanced plaques with smooth muscle cells and lipid-laden macrophages in many large aneurysms. They also reported that it was often difficult to separate the atherosclerotic region from the rest of the wall.

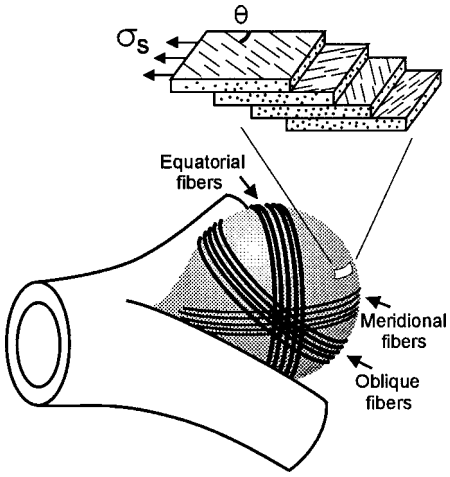

Figure 2. Schema of a saccular lesion showing overlapping layers of collagen fibers of different strengths. The inset illustrates how the alignments in adjacent layers combine to give tensile strength σ_s (modified from [66]).

The main characteristic of the aneurysm wall is its multidirectional collagen fibers – at physiological pressures they become straight and thereby govern the overall stiffness of the lesion (Figure 2). As the aneurysm enlarges, collagen is repeatedly synthesized and degraded; that is, the architecture evolves "continuously". Three important parameters are changes in the orientation, cross-linking, and volume fraction of the various types of collagen. For example, type I collagen is substantially stiffer than type III, and the alignment of the collagen fibers is fundamental to the strength of the tissue that must bear biaxial loading. Thus, there is a need for combined histo-mechanical analyses.

Most general microscopic studies of the aneurysmal wall have been on lesions that were not fixed at arterial pressure. In the unloaded state, the collagen fibers are wavy, and their preferred orientations are not discerned easily when viewed using normal stains for light microscopy. Since collagen is birefringent, however, polarized light can be used to identify the collagen and to assess its orientation [104, 106] Results by our group that exploit these observations are presented below in the sub-section on collagen architecture.

4. Assessments of Mechanical Behavior

Scott et al. [83] performed *in vitro* pressure-volume tests on seven human saccular aneurysms obtained at autopsy. Data were reduced assuming that the lesions were perfect spheres, having deformed volumes of $4\pi a^3/3$; this allowed them to estimate the deformed radii a and wall tension $T = Pa/2$ (using Laplace's relation for a thin-walled pressure vessel). Scott et al. reported that aneurysms exhibit a nonlinear behavior over finite strains, and suggested that they are stiffer

than normal vessels. They also reported that two aneurysms exhibited a critical breaking (Cauchy) stress σ_c on the order of 2 to 3 MPa. Because they measured global volumes, not local strains, the results are both averaged and effectively one-dimensional and consequently not sufficient for quantifying the requisite multiaxial constitutive relations.

Steiger et al. [93] reported results from uniaxial extension tests on thin strips of tissue excised from six human saccular lesions. Important findings are that lesion behavior differs at the fundus and neck: tearing occurred at a stretch $\lambda = 1.37$ and a stress $\sigma_c = 0.5$ MPa in the fundus and $\lambda = 1.57$ and $\sigma_c = 1.2$ MPa in the neck. That strain, not stress, was a more consistent metric of failure is consistent with results on the failure of arteries (see [45]). Nevertheless, Steiger's study is limited because the data were reduced using the linearized measure of strain, and based on the overall length of the specimen rather than a central gage length. Moreover, the 1-D data did not discriminate between the meridional and circumferential behaviors. Toth et al. [97] recently reported similar uniaxial data from 22 human aneurysms, including 17 harvested at surgery. The characteristics of the latter group includes a mean diameter of 11.6 mm (ranging from 5 to 23 mm) and a mean patient age of 47 years old (range from 32 to 63). Twelve of the 17 lesions were from females, and 11 of the 17 patients had a history of *SAH*. Similar to Steiger et al., it was found that (circumferentially oriented) specimens from the fundus tore at lower stretches (i.e., $\lambda = 1.23$) than those from the neck ($\lambda = 1.55$). Moreover, the strength near the fundus was greater in the meridional than the circumferential direction. Additional results were presented in terms of moduli for a Kelvin–Voigt linear viscoelastic model; use of a linearized measure of strain is clearly inappropriate given the reported stretches up to 55%. Remarkably, these three studies represent the entirety of the data up to 1999 on the mechanical behavior of human saccular aneurysms. The need for experimental data and the associated constitutive formulations is clear therefore.

In summary, histopathology and mechanical tests reveal the following general characteristics of "non-complicated" saccular aneurysms: they are thin-walled shell-like structures that consist primarily of a 2-D plexus of collagen, they appear to have negligible bending stiffness, they exhibit nonlinear anisotropic pseudoelastic responses over finite strain, and their properties vary regionally. Clearly, therefore, a nonlinear membrane theory is a reasonable starting point for analysis. Although Scott's data are not sufficient for detailed quantification of multiaxial behavior, including anisotropy and heterogeneity, Kyriacou and Humphrey [57] showed that they are well described by a Fung-type pseudostrain-energy function w, which is defined per undeformed surface area consistent with the direct membrane approach [47]. That is, consider a w of the form

$$w = c[\mathrm{e}^{Q} - 1], \quad Q = c_1 E_{11}^2 + c_2 E_{22}^2 + 2c_3 E_{11} E_{22}, \tag{1}$$

where E_{AB} are the principal (in-plane) Green strains and c and c_i are material parameters. For the quasi-static inflation of a perfectly spherical membrane (as

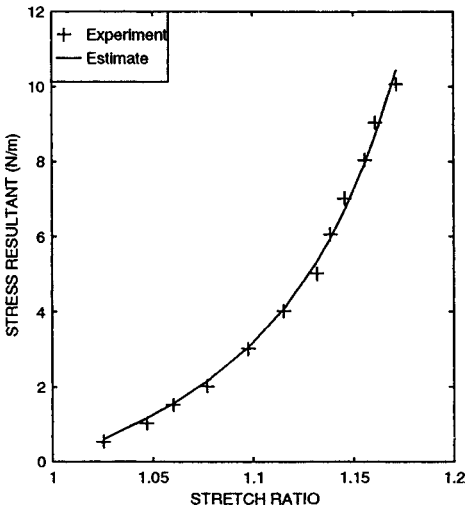

Figure 3. Best-fit of equation (1) to the tension-stretch data of Scott et al. (from Kyriacou and Humphrey, with permission).

assumed by Scott et al.), the 2-D deformation gradient is $\mathbf{F} = \text{diag}[\lambda, \lambda]$ where $\lambda = a/A$ (with A the undeformed radius) and the principal Green strains are $E_{11} = E_{22} = \frac{1}{2}(\lambda^2 - 1)$. Recalling the general constitutive relation for a membrane,

$$T_{\alpha\beta} = \frac{1}{\det \mathbf{F}} F_{\alpha\Delta} F_{\beta\Xi} \frac{\partial w}{\partial E_{\Delta\Xi}}, \quad \alpha, \beta, \Delta, \Xi = 1, 2, \tag{2}$$

with $c_2 \equiv c_1$ due to the implicit assumption of in-plane isotropy in Scott's analysis, we see that the uniform tension $T (= T_1 \equiv T_2)$ is

$$T = c\Gamma(\lambda^2 - 1) \exp[0.5\Gamma(\lambda^2 - 1)^2], \tag{3}$$

where $\Gamma \equiv (c_1 + c_3)$. Kyriacou and Humphrey determined the best-fit values of the two independent material parameters c and Γ via a Marquardt–Levenberg regression of the data presented by Scott et al., that is by minimizing the sum-of-the-squares of the error between the calculated and measured tensions (i.e., stress resultants). The best-fit values were $c = 0.88$ N/m and $\Gamma = 12.99$, which yielded the fit to data shown in Figure 3. Despite this good fit, the inadequacy of the data is evident: they do not allow separate determination of c_1 and c_2, which embody the material symmetry, they do not separate the contributions due to c_1 and c_3, and they do not provide information on possible heterogeneities. Based on results on arteries reported by Fung and colleagues, Kyriacou and Humphrey assumed that $c_3 \sim c_1/10$, and hence $c = 0.88$ N/m, $c_1 \equiv c_2 = 11.82$ and $c_3 = 1.18$. Likewise, various anisotropies can be explored by varying the values of c_1 and c_2 (see Section 7).

5. Hypothesized Mechanisms of Enlargement and Rupture

5.1. LIMIT POINT INSTABILITIES

A longstanding question with regard to saccular aneurysms has been, how can a structure that consists of collagen, which exhibits high stiffness and low extensibility, continue to enlarge and eventually rupture? In an effort to address this question, Austin et al. [6] and Akkas [1] suggested that saccular aneurysms suffer limit point instabilities, that is (mathematical) bifurcations in their quasi-static response to increases in distension pressure. Note, however, that Austin et al. based their conclusions on *in vitro* experiments on a "model lesion" that they constructed by gluing a 0.8 mm thick collagen patch onto the center of a 0.175 mm thick elastomeric membrane that was fixed around its periphery and inflated from underneath. Because of the use of the elastomeric membrane, it is to be expected that this model exhibited a limit point instability [8]. Akkas, on the other hand, reported computational results for the inflation of a neo-Hookean model (i.e., $W = c(\mathrm{tr}\,\mathbf{C} - 3)$, where $\mathbf{C} = \mathbf{F}^{\mathrm{T}}\mathbf{F}$) of a saccular aneurysm, which also exhibited a limit point as expected. Because aneurysms, like most collagenous soft tissues, tend to exhibit an exponential rather than rubber-like behavior, it is clear that these studies needed to be revisited.

Consider an idealized spherical lesion⋆ having an undeformed radius A, a uniform initial thickness H, and subjected to a uniform distension pressure P. With $\mathbf{F} = \mathrm{diag}[\lambda, \lambda]$, is it easy to show that the pressure-stretch relation for the Fung-type form of w (equation (1)) is

$$P(\lambda) = \frac{2c\Gamma}{A}\big(\lambda - 1/\lambda\big)\exp[0.5\Gamma(\lambda^2 - 1)^2], \tag{4}$$

which is easily non-dimensionalized by multiplying $P(\lambda)$ by A/c. Regardless, a limit point exists if $\mathrm{d}P/\mathrm{d}\lambda = 0$ for any $\lambda > 1$ (note: a membrane cannot support compression, thus the restriction on λ). It can be shown numerically that the Fung material does not admit a limit point, with $\Gamma = 12.99$ from Scott's data. Inasmuch as Kyriacou and Humphrey [57] found a similar result for a more general case of an axisymmetric lesion (using finite elements), it appears that certain sub-classes of saccular aneurysms probably do not enlarge or rupture via a limit point instability. This finding re-emphasizes the importance of basing one's analysis on appropriate constitutive relations.

5.2. DYNAMIC INSTABILITIES

Richardson and Kofman [77] reported bruits in cerebral aneurysms – that is, audible tones at frequencies ∼400 Hz. Ferguson [23] suggested that these bruits

⋆ Shah et al. [84] showed that the spherical assumption is reasonable for a small sub-class of aneurysms.

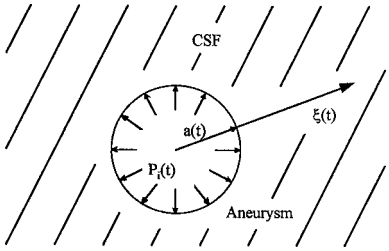

Figure 4. Schema of a spherical aneurysm surrounded by cerebral spinal fluid. The radial coordinate defining the fluid domain is $\xi \in [a(t), \infty)$ (from Humphrey, with permission).

resulted from turbulence within the lesion while others suggested that they indicated that aneurysms are excited at their natural frequency [50, 81, 86]. Resonance implies large wall motions, indeed violent vibrations, and thus was hypothesized by some as a potential mechanism of enlargement or rupture. There have been but a few analyses of the associated elastodynamics, however, most of which are based on classical shell theory and thus linearized strains and material behavior (e.g., [49, 86]). Moreover, none of these studies account for the observation that many saccular aneurysms are surrounded by cerebral spinal fluid (*CSF*). Below, we summarize a recent study by Shah and Humphrey [85] that is based on finite elasticity and accounts for the *CSF*. First, however, it is important to note the following findings from hemodynamic studies. Experimental and computational results both reveal that flow-induced wall shear stresses τ_w are small in all classes of saccular aneurysms studied to date: maximum values are ~5 to 13 Pa [65, 94], which are less than the 40 Pa needed to induce endothelial cell damage [30] and orders of magnitude less than the pressure-induced in-plane wall stresses which can be 1 to 10 MPa [12, 57]. These findings, coupled with observations that the maximum wall shear stress typically occurs at the neck, not the fundus where rupture tends to occur, suggest that intra-aneurysmal pressures are the dominant hemodynamic loads governing stress-induced rupture [29, 80, 94]. This is not to say that wall shear stresses are not important; they likely signal the endothelium to express various molecules, including growth factors that may regulate the intramural collagen. This latter role has not been explored in detail, though it ought to be. It also appears that intra-aneurysmal pressures are similar in magnitude to those in the parent vessel [16, 25, 67, 81] and that they vary little with position within the lesion [33, 37]. Consequently, it appears to be reasonable to assume (to first order) that saccular aneurysms are loaded primarily by a uniform, time-varying distension pressure.

For purposes of examining the elastodynamics, consider a thin-walled, spherical aneurysm of initial radius A and wall thickness H, but now let it be subjected to a time-varying distension pressure $P_i(t)$ and surrounded by *CSF* (Figure 4). The 2-D deformation gradient tensor $\mathbf{F} = \text{diag}[\lambda(t), \lambda(t)]$, where $\lambda(t) = a(t)/A$ and $a(t)$ are the deformed radii. In addition, let the lesion exhibit an isotropic, Fung-type

behavior (equation (1)). From Kraus [56], it can be shown that the three equations of motion for a membrane reduce to a single ordinary differential equation for a pulsating sphere:

$$\rho h \frac{\mathrm{d}^2 u_r}{\mathrm{d}t^2} = -2T\kappa - t_{rr}(r_i) + t_{rr}(r_o), \tag{5}$$

where ρ is the mass density of the aneurysm, $h(t)$ is the deformed thickness (which equals $H/\lambda(t)^2$ if incompressible), $u_r(t) = a(t) - A$ is the radial displacement, $T = T(\lambda)$ is the constitutively determined wall tension, $\kappa(t) = 1/a(t)$ is the curvature in the deformed configuration, and t_{rr} are radial stresses on the inner and outer surfaces of the lesion. Assuming a prescribed time-varying uniform luminal pressure, $t_{rr}(r_i) = -P_i(t)$, Milnor [68] shows that arterial pressures are well described by a Fourier series representation of the form,

$$P_i(t) = P_m + \sum_{n=1}^{N} \big(A_n \cos(n\omega t) + B_n \sin(n\omega t)\big), \tag{6}$$

where P_m is the mean blood pressure, A_n and B_n are Fourier coefficients for N harmonics, and ω is the circular frequency. Ferguson [25] reported micro-catheter measured intra-aneurysmal blood pressures in humans. From these data, it can be shown that specific values of A_n and B_n, for the first 5 harmonics, are $A_1 = -7.13$, $B_1 = 4.64$, $A_2 = -3.08$, $B_2 = -1.18$, $A_3 = -0.130$, $B_3 = -0.564$, $A_4 = -0.205$, $B_4 = -0.346$, $A_5 = -0.0662$, and $B_5 = -0.120$, all in mmHg, with $P_m = 65.7$ mmHg. Note that these lower pressures were recorded in supine, anesthetized patients.

The cerebral spinal fluid (*CSF*) could similarly be assumed to exert a uniform time-varying pressure $P_o(t)$ on the outer surface of the membrane that is a reaction to the pressure-induced distension of the lesion. This is tantamount to treating the *CSF* as an ideal fluid (i.e., inviscid and incompressible). In this case, $t_{rr}(r_o) = -P_o(t)$, where P_o can be determined by solving the pressure field in the fluid domain $\xi \in [a, \infty)$. For an ideal fluid, the governing differential equations are the balance of mass and linear momentum (i.e., Euler) equations. In the absence of body forces, they can be written as $\nabla\cdot\mathbf{v} = 0$ and $-\nabla P = \rho_f \mathbf{a}$, respectively, where $\mathbf{v}$ and $\mathbf{a}$ are the fluid velocity and acceleration and ρ_f is the mass density of the *CSF*. It is probably better to assume that the *CSF* is viscous (e.g., Newtonian), however. In this case, the governing differential equations are the balance of mass and the incompressible Navier–Stokes form of the linear momentum equations ($-\nabla P + \mu\nabla^2\mathbf{v} = \rho_f \mathbf{a}$), and the outer stress boundary condition is $t_{rr}(r_o) = -P_o(t) + 2\mu D_{\xi\xi}(\xi_o)$ where $\mathbf{D}$ is the stretching tensor ($\mathbf{D} = \frac{1}{2}(\mathbf{L} + \mathbf{L}^{\mathrm{T}})$, where $\mathbf{L}$ is the velocity gradient tensor). Because the solution for the ideal fluid can be recovered from that for the Newtonian fluid, we consider the latter here.

Assuming a flow in the radial direction ξ in a spherical domain (Figure 4), mass balance requires that

$$\frac{1}{\xi^2}\frac{\partial}{\partial \xi}\left(\xi^2 v_\xi\right) = 0 \rightarrow v_\xi(\xi, t) = \frac{g(t)}{\xi^2}, \tag{7}$$

where the function $g(t)$ is determined by requiring a material particle on the membrane to have the same velocity as the adjacent fluid particle v_ξ. Hence, at $\xi = a$,

$$\frac{\mathrm{d}}{\mathrm{d}t}\left(u_r\right) = \frac{\mathrm{d}\lambda}{\mathrm{d}t}A = \frac{g(t)}{a^2} \rightarrow g(t) = A^3\lambda^2\frac{\mathrm{d}\lambda}{\mathrm{d}t}. \tag{8}$$

The requisite component of **D** is thus computed easily.

For this radial flow, the meridional and circumferential Navier–Stokes equations require that the fluid pressure $P = P(\xi, t)$ alone. Hence, the only "non-trivial" equation of motion is the radial one, which can be integrated over $\xi \in [a, \infty)$ to yield the pressure $P_o(t)$ exerted on the outer surface of the membrane by the surrounding CSF:

$$P_o(t) = P_\infty(t) + \rho_f A^2\left(\lambda\frac{\mathrm{d}^2\lambda}{\mathrm{d}t^2} + \frac{3}{2}\left(\frac{\mathrm{d}\lambda}{\mathrm{d}t}\right)^2\right), \tag{9}$$

wherein we have used v_ξ from mass balance and the matching condition at the solid-fluid interface. It is interesting to note that this is the same pressure field as that for an ideal fluid (i.e., as that obtained by integrating the unsteady Bernoulli equation along a radial streamline).

Taken together, these equations yield the final governing differential equation [85]:

$$\left(\frac{\rho HA}{\lambda^2} + \rho_f A^2\lambda\right)\frac{\mathrm{d}^2\lambda}{\mathrm{d}t^2} + \frac{3}{2}\rho_f A^2\left(\frac{\mathrm{d}\lambda}{\mathrm{d}t}\right)^2 + \frac{4\mu}{\lambda}\frac{\mathrm{d}\lambda}{\mathrm{d}t} + \frac{2T(\lambda)}{A\lambda} = P_i(t) - P_\infty(t) \tag{10}$$

with $T(\lambda)$ given by equation (3) and $P_i(t)$ by equation (6). This nonlinear second-order ordinary differential equation can be solved using numerical techniques such as Runge–Kutta, which is facilitated by transforming it into a system of two first-order equations (this is simplified by first non-dimensionalizing the equation). Shah and Humphrey [85] solved this system of equations for the following values of parameters, which they suggested define a representative lesion: $\rho = 1050$ kg/m^3, $A = 3 \times 10^{-3}$ m, $H = 27.8 \times 10^{-6}$ m, $\rho_f = 1000$ kg/m^3, $\mu = 1.26 \times 10^{-3}$ Ns/m^2, $P_\infty = 3$ mmHg, and $c = 0.88$ N/m, $c_1 = c_2 = 11.82$, and $c_3 = 1.18$. See the original paper for complete results. Figure 5, panel B shows that equilibrium initial conditions yield a periodic solution as expected (i.e., a closed path in the phase-plane); panel C reveals further that, for the case of perturbed initial conditions, this periodic solution serves as an attractor (i.e., the oscillations tend to dissipate

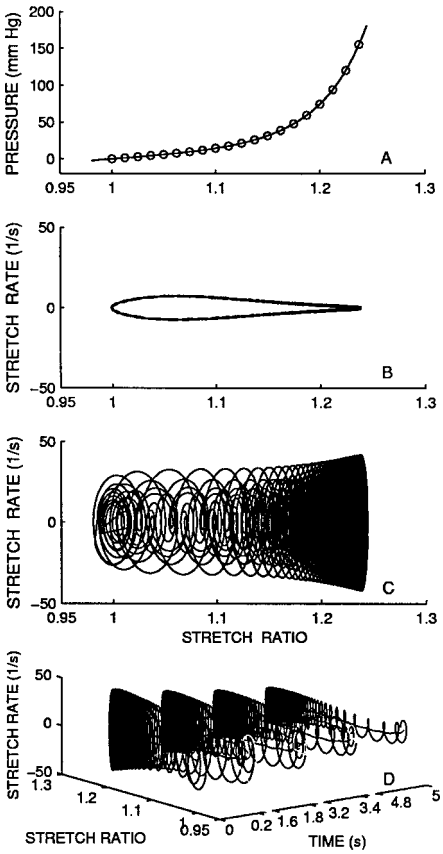

Figure 5. Results from Shah and Humphrey on the elastodynamics of a saccular aneurysm subjected to a sinusoidal forcing (pressure) function. Panel B shows the periodic solution in the unperturbed case, and panels C and D show that this solution is an attractor in the case of perturbed initial conditions, thus suggesting dynamic stability (from Shah and Humphrey, with permission).

and the perturbed solution returns to the periodic solution) and hence the solution is dynamically stable. Additional results suggest that the time-dependent solution can be treated quasi-statically as a series of equilibria. Whether this observation holds for other situations (e.g., different material parameters, different geometries, different forcing functions, etc.) must be examined individually, and remains an open problem. Based on this simple analysis, however, it appears that at least one sub-class of (nearly) spherical saccular aneurysms is dynamically stable both when $P_i(t)$ is a periodic function having a fundamental frequency less than 5–10 Hz (the non-autonomous system) and when it is a constant (the autonomous system; not shown). It appears reasonable, therefore, to emphasize quasi-static stress analyses for insight into the mechanics, a conclusion supported by Steiger [95]. Indeed, because saccular aneurysms are known to be thin, membranous tissues subject to

low frequency pulsatile pressures, intuition suggests that the inertial effects would be small.

5.3. STRESS ANALYSES

There have been few rigorous studies of the quasi-static response of the aneurysmal wall to applied loads. Overly simplified analyses have been based on electrical analog models of latex balloons [5, 19] or constitutive relations that describe the behavior of rubber-like [1] or linear materials [34, 86] – (note: [34] is based on an incorrect equilibrium solution using a so-called modified Laplace's equation).

Laplace's equation $T = Pa/2$ is a universal solution for a thin-walled sphere and thus is applicable to saccular aneurysms (as used in the above limit point analysis). Canham and Ferguson [12] used Laplace's equation to estimate a critical diameter d_c at which a lesion may rupture. They assumed that the aneurysmal tissue volume v_T $(= 4\pi a^2 h)$ remains constant at all transmural pressures P (i.e., that these lesions suffer isochoric motions in a given state of enlargement), and showed that

$$d_c = \left(\frac{4\sigma_c v_T}{\pi P} \right)^{1/3}, \tag{11}$$

where σ_c is a critical wall strength. Rough estimates of $v_T = 1$ mm^3, $\sigma_c = 10$ MPa (recall that Scott et al. reported a $\sigma_c = 1$–2 MPa and Steiger et al. reported a $\sigma_c = 0.5$–1.2 MPa, both from uniaxial studies), and $P = 150$ mmHg suggested a $d_c = 8.6$ mm, a reasonable value. Limitations of this approach are the same as those in the work of Humphrey and Kyriacou [46] and Shah and Humphrey [85] – assumption of homogeneous and in-plane isotropic tissue behavior as well as homogeneity of the calculated stress and strain fields. The latter suggests that each material point is equally likely to fail, which does not account for the propensity of rupture at the fundus [18, 80, 92].

Despite the usefulness of simple spherical models, more realistic analyses are needed to account for the complex geometry, material properties, and applied loads that characterize the mechanics of an intracranial saccular aneurysm. Towards this end, Kyriacou and Humphrey [57] and Shah et al. [84] solved the equilibrium problem in weak form using the finite element method. For example, one can solve nonlinear axisymmetric and nonaxisymmetric inflation problems using the principle of virtual work,

$$\int_{\Omega_o} \delta w \, \mathrm{d}A - \int_{\Omega} P\mathbf{n} \cdot \delta\mathbf{x} \, \mathrm{d}a = 0, \tag{12}$$

where w is the 2-D strain-energy function, P the distension pressure, $\mathbf{n}$ an outward unit normal to the membrane in the current configuration Ω, $\delta\mathbf{x}$ the virtual changes in position, and Ω_o the original domain. After introduction of suitable interpolation functions and numerical integration via appropriate quadrature rules, equation (12)

reduces to a system of nonlinear algebraic equations of the form $\mathbf{g}(\mathbf{q}) = \mathbf{0}$, where $\mathbf{q}$ represents the vector of (unknown) nodal positions. This equation admits an iterative Newton–Raphson solution, viz.

$$\mathbf{K}(\mathbf{q}^i)[\mathbf{q}^{i+1} - \mathbf{q}^i] = -\mathbf{g}(\mathbf{q}^i), \tag{13}$$

where $\mathbf{K} = \partial\mathbf{g}/\partial\mathbf{q}$ is the tangent matrix and i an iteration counter. This finite element solution thereby yields the current position of each node, from which one can compute strains and then stresses; this allows one to quantify the heterogeneous and anisotropic response of aneurysms to distention pressures. Kyriacou and Humphrey [57] and Shah et al. [84] considered a class of idealized axisymmetric saccular aneurysms having an initially uniform wall thickness H, a truncated spherical or elliptical geometry, a Fung-type constitutive behavior, and a clamped boundary condition at the neck. Not having sufficient data to quantify possible regional variations in material behavior, they considered a range of stress–strain behaviors from isotropic and homogeneous to anisotropic and heterogeneous. Using the aforementioned results for equation (3) and Scott's data, they defined isotropic behavior by $c = 0.8769$ N/m, $c_1 = c_2 = 11.82$, and $c_3 = 1.18$. For anisotropic behavior, the values of c and c_3 were the same, but values of c_1 and c_2 were modified to allow the ratio c_1/c_2 to vary linearly with the undeformed arc length $S \in [0, L]$ from $c_1/c_2 = 1$ at the fundus ($S = 0$) to either 3 or $1/3$ at the neck ($S = L$). Kyriacou and Humphrey prescribed the variation in c_1/c_2 such that the value of $w\,(\lambda_1 = 1.18, \lambda_2 = 1.18)$ was the same at the neck as it was in the isotropic case; Shah et al. ensured that $w\,(\lambda_1 = 1.18, \lambda_2 = 1.18)$ remained the same at each point. Whereas the former allows regional variations in material heterogeneity (as suggested by the data of Steiger et al. [93]) and material symmetry, the latter maintains a type of homogeneity and thereby isolates effects of regional variations in symmetry. Of course, c_1/c_2 must equal 1 at the fundus due to axisymmetry, which requires $T_1 = T_2$ and $\lambda_1 = \lambda_2$ at that location. Finally, the prescribed boundary conditions were zero displacement at the neck (i.e., $u_r = 0$ and $u_z = 0$ at $z = 0$, which enforces $\lambda_2 \equiv 1$ at $z = 0$, where $\mathbf{u}$ is the displacement) and zero radial displacement at $r = 0$, the symmetry axis.

Perhaps the first question that one should address with the finite element method is the applicability of the Laplace equation $T_\alpha \equiv T = Pa/2$. Shah et al. [84] attempted this by first finding the best-fit sphere for the deformed configuration of model lesions as calculated by finite elements. They fit the deformed generator curve via $(r^j)^2 + (z^j - o)^2 = a^2$, where $j = 1, \ldots, n$ is the number of nodes used in the simulation, and o and a define the center and radius of the best-fit sphere. Next, they calculated the principal uniform Cauchy stress t, which equals T/h or $T\lambda^2/H$ where $h = H/\lambda^2$ is the deformed thickness, $\lambda = a/A$ the uniform stretch ratio, and A the best-fit undeformed radius. This requires a value for the uniform λ associated with T, which was obtained by inverting the constitutive relation (cf. equation (3)). Finite element and Laplace results were then compared as a function of undeformed arc length S.

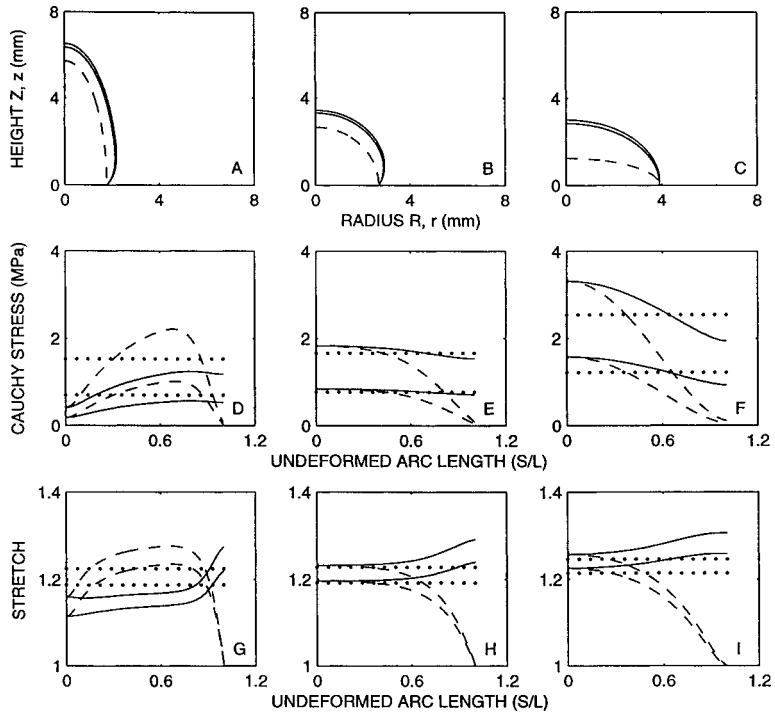

Figure 6. Finite element results for a model isotropic and axisymmetric aneurysm – $c = 0.88$ N/m, $c_1 = c_2 = 11.82$, $c_3 = 1.18$, $H = 27.8$ μm, initial volume = 0.0398 ml, and $A : B = 0.32$, 1.0, and 3.12. Panels A–C show the undeformed (dashed) and deformed (solid lines) configurations at 80 and 160 mmHg pressure. Panels D–F show the associated stresses in the meridional and circumferential directions, with the dotted lines showing the Laplace approximation. Panels G–I show the associated stretches (from Shah et al., with permission).

Figure 6 shows results for lesions having three different initial geometries (i.e., values of A/B, the ratio of the initial R and Z major axes) but otherwise the same initial lesion volume, thickness, isotropic material behavior, quasi-static distension pressure, and boundary conditions; specific values are in the figure legend. The undeformed generator curves (dashed lines in panels A to C) reveal that the prescribed geometry was one half of a complete ellipse or sphere. Panels A to C show how the initially elliptical or spherical geometry was distorted upon loading (see solid lines) due, in part, to the fixed boundary condition at the neck. Despite equal increments in pressure from 0 to 80 and then 80 to 160 mmHg, most deformation occurred at lower pressures as expected of a material that exhibits an exponential stress–strain behavior. Panels D to F reveal a number of important observations with regard to the distributions of the principal Cauchy stresses t_α: the meridional stress (solid curve) was higher than the circumferential stress (dashed curve) in lesions when $A/B \geqslant 1$, but the converse was true when $A/B < 1$; the highest multiaxial stresses occurred at the fundus in the lesions with the highest ratio of A/B; the highest multiaxial stresses occurred near $S/L \sim 0.7$ (with $S/L = 0$

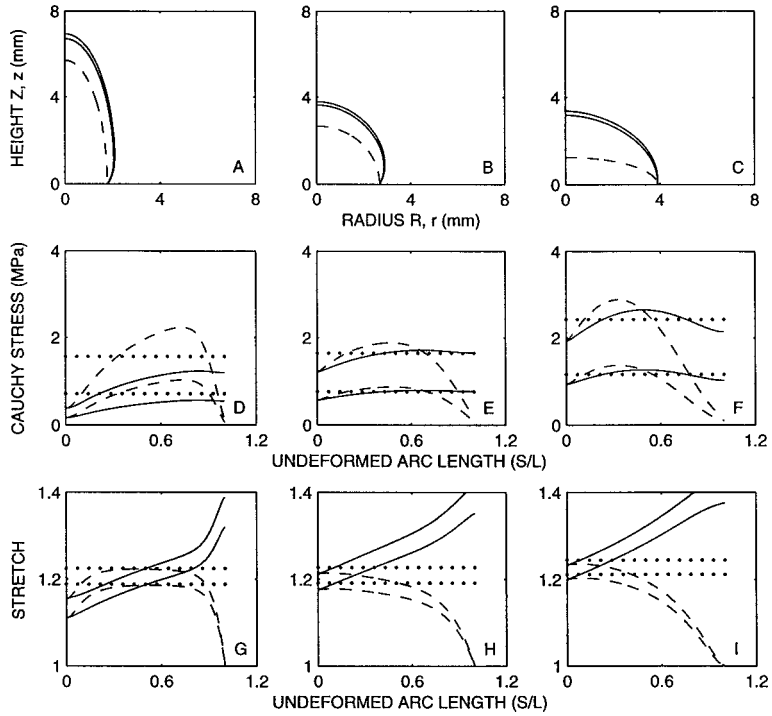

Figure 7. Similar to Figure 6 except for lesions having an increasingly greater stiffness in the circumferential direction as you move from the fundus to the neck.

at the fundus and 1 at the neck) for lesions with $A/B < 1$; and, as expected, stresses were uniform over the largest domain in lesions having $A/B = 1$ (i.e., an initially spherical geometry). Panels G to I show the associated distributions of the principal stretch ratios λ_α. Note that $\lambda_2 = 1$ at $S/L = 1$ as required by boundary conditions. The horizontal dotted lines in panels D to I show the uniform stress and stretch values predicted by the Laplace solution; recall that these were calculated based on the best-fit sphere for the deformed configuration. As expected, the Laplace approximation was best for the initially spherical geometry although one may argue that a reasonable mean value for $T_\alpha(S)$ was obtained in each case. Details on the stress field provide much greater information, however.

Additional results were reported for the same three lesions and loading conditions with the exception that the material properties varied linearly in S from isotropic at the pole (i.e., $c_1 = c_2 = 11.8$ at $S/L = 0$) to meridionally stiffer at the neck (i.e., $c_1 = 17.79$ and $c_2 = 5.93$ at $S/L = 1$). The deformed configurations were similar to those in Figure 6, and so too for the stress and stretch fields with two exceptions: the maximum stresses increased at the fundus and the meridional stretch decreased at the neck when $A/B \geqslant 1$, and the maximum values of circumferential stress and stretch (i.e., near $S/L = 0.7$) increased slightly with respect to those in Figure 6 when $A/B < 1$. Figure 7 shows results for the same three

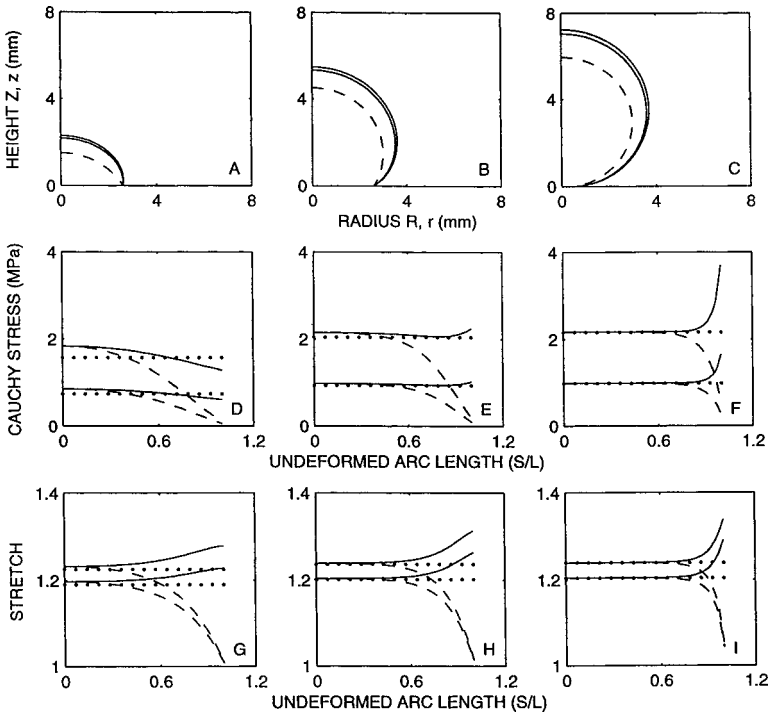

Figure 8. Similar to Figure 6 except for lesions of three different initial sizes (from Shah et al., with permission).

lesions with the exception that the material properties varied linearly in S from isotropic at the fundus to circumferentially stiffer at the neck (i.e., $c_1 = 5.93$ and $c_2 = 17.79$ at $S/L = 1$). In contrast to changes associated with the meridionally stiffer lesion, this circumferentially stiffer behavior resulted in marked differences in the stress and stretch fields, particularly when $A/B \geqslant 1$. For example, panels E and F in Figure 7 reveal that an increased circumferential stiffness resulted in a decreased equibiaxial stress at the fundus, a maximum multiaxial stress away from the fundus, and an increased meridional stretch near the neck. Increasing the circumferential stiffness when $A/B > 1$ thus tended to homogenize the stress field.

Figure 8 shows results for lesions having three different initial sizes (i.e., luminal volume) but otherwise the same initial spherical shape (i.e., the same undeformed radius, but truncated at different locations), thickness, isotropic material behavior, quasi-static distension pressures, and boundary conditions. As expected, panels A to C show that the more completely spherical geometry (panel C) yielded the most sphere-like behavior; that is, the stress and stretch fields are uniform and equibiaxial over a large portion of the lesion, the only variations being due to the boundary condition at the fixed neck (a boundary layer effect). Despite marked differences in size (undeformed and deformed), the magnitude of the stresses and stretches were nearly the same at the fundus and similar over the entire domain.

This was anticipated for the general solution for the inflation of an axisymmetric membrane is [47],

$$T_1 = \frac{P}{2\kappa_2}, \qquad T_2 = \frac{P}{\kappa_2}\left(1 - \frac{\kappa_1}{2\kappa_2}\right), \tag{14}$$

which reveals that it is the principal curvatures (κ_α), not the size per se, that controls the stress resultants – this has not yet been appreciated clinically as noted earlier with regard to the ongoing search for the "critical size". Finally, the dotted lines reveal, as expected, that a Laplace approximation is reasonable for nearly complete sphere-like lesions (panels B and C) but less good for cap-like lesions.

Despite longstanding reliance on the maximum dimension as a predictor of rupture-potential, this metric has failed to answer the most important clinical questions: Why do some lesions expand whereas others remain dormant for long periods? Why do some lesions rupture whereas most do not? Why does rupture tend to occur at the fundus even when the neck is thinner? Although based on incomplete data, the biomechanical analyses presented here reveal important insights that address these questions in part. It appears that lesions do not enlarge because of material or dynamic instabilities; it appears that the local curvature and anisotropic material properties, not lesion size, govern the distribution of intramural stress; and it appears that the stresses are greatest at the fundus if the material behavior is either isotropic or meridionally stiffer (recall that Toth et al. [97] found the latter experimentally).

6. Need for a Structurally-Based Constitutive Relation

The above results demonstrate that biomechanics can and must play a role in understanding better the natural history of saccular aneurysms and their treatment. Yet, analyses are only as good as the data upon which they are founded. A pressing need in aneurysm research is the identification of an improved stress–strain relation for the tissue. It is axiomatic that material behavior results from the internal composition of the material, hence an appropriate starting point is quantitative histology.

6.1. COLLAGEN ARCHITECTURE

Collagen is a highly structured cross-linked biopolymer, able to withstand high tensile loads. Tendon, having type I fibers, is perhaps the simplest and most thoroughly studied collagenous tissue; it has a breaking strength of 60–100 MPa and a stiffness of 1.0–2.5 GPa at its maximum extension [22, 101]. A collagenous framework provides strength and stiffness to blood vessels as well. Many arteries are able to withstand more than 10× the normal blood pressure. Even veins, which may be tested to pressures approaching 600 mmHg prior to use as bypass vessels for the heart, are exceptionally strong [2]. That intracranial saccular aneurysms

rupture suggests that they are, in contrast, much less able to withstand the persistent loads due to normal physiological or pathological blood pressures (e.g., up to ∼200 mmHg). It appears that two aspects of collagen structure may be key to the reduced strength of saccular aneurysms – the layered organization of the fibers within the wall and the existence of a fiber complement that is substantially weaker than normal type I collagen [7, 14, 15, 31, 69].

The general spherical shape of saccular aneurysms provides a basis for understanding the load carrying capability of the wall. Arterial blood pressure stresses the wall of a spherical lesion equally in all tangential directions, with "modest" differences in the stresses for elongated or flattened lesions [57]. Of course, more varied forms of saccular aneurysms, with secondary lobes on the primary lesion or biloculations, will have a correspondingly varied distribution of wall stresses. There is a need to correlate structure and mechanics in saccular aneurysms as attempted in other collagenous tissues (e.g., see [22, 63, 64]). Moreover, new results are needed to understand better how the aneurysmal wall behaves in the short term as a stiff elastic collagenous fabric, whereas over the longer term, it behaves *in vivo* as a remodeling, irreversibly enlarging structure. Progress has been made by applying multi-dimensional polarized light (MDPL) microscopy, which has the potential to complement the tissue mechanics. The key to assessing directional tissue properties is an evaluation of the directional distribution of the constituent fibers, layer by layer, and quantification of the proportion of fibers in each direction as well as their uniaxial strength within each layer.

Given that the aneurysmal wall consists primarily of collagen, it is useful to exploit the birefringent optical properties of individual collagen fibers – wherein the morphological, mechanical, and optical axes coincide – to study both orientation and distribution with the polarizing microscope [9]. The histological processing for such studies is standard (i.e., fixation, dehydration, paraffin infiltration and embedding, and subsequent sectioning via a microtome), except for the staining of tissue after sectioning. Birefringent enhancement stains make the measurement of the alignment of individual fibers more precise [87] and they make possible a measure of the strength of birefringence from the same local region. Thus, there are two polarized light techniques of importance in studying aneurysmal collagen: the Universal Stage attachment enables measurement of orientation in three dimensions and the Senarmont compensator, which is a 45 degree aligned quarter-wave filter, allows measurement of the birefringence of individual fibers [9].

The Universal Stage is an effective instrument for measuring two fiber angles: the azimuth, in the plane of the tissue section, and the elevation, measured out of the plane of the section. Thus, the tissue section is viewed optically as a thick transparent section and the birefringent collagen fibers within that section reveal their 3-D alignment directly on the polarizing microscope. A key point is that the inner stage of the instrument containing the tissue slide is mounted so that it can be rotated freely in three dimensions up to a tilt angle of 50°. Measurements of alignment are made at extinction, which has a precision of approximately $\pm 1°$

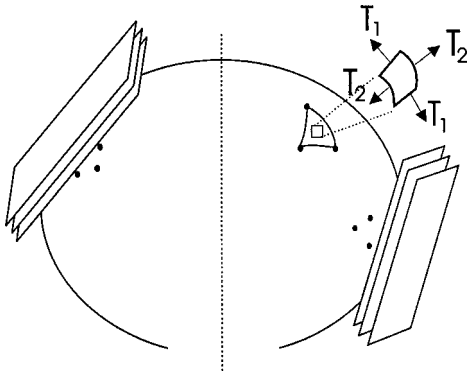

Figure 9. Schema to illustrate several tangential sectioning planes on the surface of an aneurysm. The local stretches and stress resultants can be assessed separately in each region prior to perfusion fixation.

[87]. Graphical presentation and analysis of data have been accomplished using the Lambert equal area projection.

Plane polarized light traversing a birefringent material is resolved into two rays, the *ordinary ray* and the *extraordinary ray*, which vibrate at right angles to each other and travel at different velocities. The velocity difference introduces a phase difference between the two rays that depends directly upon the strength of birefringence and the thickness of birefringent fabric. By means of the Senarmont compensator, one is able to measure, fiber by fiber, the phase difference (or phase retardation) directly on the microscope. The rationale behind the phase retardation method is that both the mechanical strength of the tissue and its birefringence depend on the cross-linked molecular structure and size of the fibers [21, 100].

An important requirement for combining both phase retardation and 3-D orientation is that the elevation angles of the measured fibers be relatively low, less than 15°, which ensures that the phase retardation is not biased toward lower values. This requirement has been met in studies on saccular aneurysms by confining analysis to tissue sections cut tangentially or near tangentially. By the method of repeated embedding, after each short series of tangential sectioning from the surface, it has been possible to retrieve collagen-related microscopic data from several regions of interest on the aneurysm surface [15]. This approach has set the stage for matching, in the future, wall structure and material behavior, region by region on individual lesions (Figure 9).

Figure 10 shows a tangentially cut section close to the luminal edge of a 2.6 mm diameter human aneurysm. Superimposed on the section are four radially aligned corridors that provide a gray-scale comparison of the strength (i.e., level) of birefringence as a function of position across the wall. The layering of the wall is evident by the concentric rings, with a parallel alignment of fibers within individual layers. The azimuthal direction of the fibers is generally coherent within layers with the mean direction varying widely from layer to layer (cf. Figure 2).

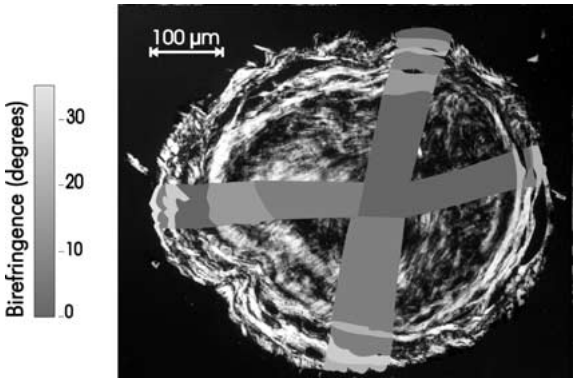

Figure 10. Polarized light micrograph of a tangential section from a 2.6 mm diameter aneurysm revealing the layered structure of the aneurysm wall (wall thickness 70 μm). Four measurement corridors are shown, with the birefringence levels of collagen within each of the layers being gray-scaled (from MacDonald et al. [66], with permission).

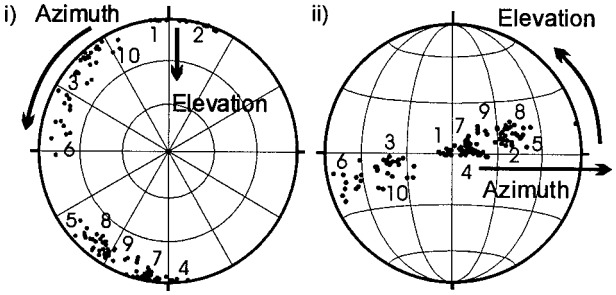

Figure 11. Lambert projections to show the orientation of collagen fibers for one of the measurement corridors from the aneurysm shown in Figure 10: (i) primary data with each layer identified by number, and (ii) data rotated to show the great circle distribution, indicating that there is a full range of directional alignments of the collagen fibers at that region on the aneurysm wall (with permission).

This distinctly layered organization has been characteristic of each of the several saccular aneurysms studied, regardless of size, provided the wall is relatively free of atherosclerosis [13, 14]. The defining feature of each layer has been primarily the mean fiber orientation, although fiber size and birefringence also contribute to the distinctiveness among layers.

Graphical presentation of directional data on Lambert projections provides a quantitative and comprehensive overview of the directional organization of the fibers in a tissue section. It is the preferred graphical method for three-dimensional data because it is an equal area projection, preserving the total area of the data regardless of its mean orientation and thus its projection position on the graph [76, 88]. Figure 11(i) is an example of a Lambert projection showing a single corridor of measurements with 10 layers across the wall of the aneurysm from Figure 10. This projection shows the clustering of the primary data around the

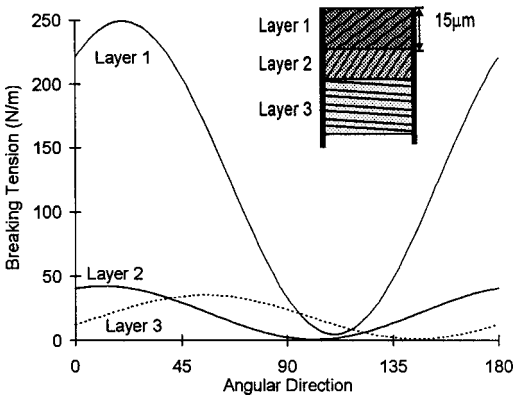

Figure 12. Plot of the calculated breaking tension in the three outer layers of an aneurysm against the angular direction of the wall, where 0° on the abscissa is the meridional direction (neck to fundus) and 90° is the equatorial direction. The inset is a schema of the three outer layers with the mean collagen orientation shown, and the gray scale indicating the strength of birefringence (from MacDonald et al., with permission).

perimeter (azimuthal directions ranging from 0 to 360°) with the elevation angle varying nonlinearly toward the center of the plot. The layers are numbered from the lumen, as layer 1, to the outer edge of the aneurysm. The computer rotated projection (Figure 11(ii)) shows the distribution of the same data relative to a great circle girdle distribution, and reveals how well these data span all orientations relative to the aneurysm surface.

Together, fiber direction and distribution provide a basis for estimating tissue strength (which also depends on cross-linking, etc.), and they can be used to develop microstructural methods such as those of Lanir [62]. The observed variation of birefringence across the aneurysm wall has suggested that it is reasonable to combine retardation and orientation data to assess directional strength of the tissue [15]. Early findings suggest that enlargement of an aneurysm requires a reorganization of the higher strength outer fibers while new collagen is added to the inner layers. Note, therefore, that several studies have linked collagen birefringence, mechanics, and the healing process – for example, in skin wound healing and maturation of a scar post myocardial infarction [21, 105, 106]. It was the study of Doillon, however, that provided the first quantitative measure of tissue strength directly from birefringence. Recently, MacDonald et al. [66] reanalyzed the data of Doillon by plotting tensile strength σ_s (kPa) versus fiber birefringence B (phase retardation in units of nm), which revealed a nonlinear relation $\sigma_s = 0.304B^{2.33}$, for which the correlation coefficient $r = 0.99$. This strength was defined as the tensile stress at which the dermal scar began to fail due to damage and/or micro-tearing. Figure 12 shows the contribution to directional strength of three outer layers of a 9 mm diameter aneurysm, and the marked differences in strength contribution because of layer thickness and fiber birefringence; included in the calculations were aneurysm radius, layer thickness, and number of layers, and the variables

of fiber alignment, birefringence, and estimated local wall thickness [66]. The data revealed a tissue anisotropy of approximately $2\times$ for the direction of least to greatest strength, with a tensile strength (in the weakest direction) ranging from 0.73 to 1.8 MPa over 4 aneurysms. Recall that Steiger et al. and Toth et al. reported direct measurements of tensile strength from aneurysmal tissue strips 0.5 MPa ± 0.26 (SE) and 0.5 to 1.45 MPa, respectively – this shows a good correspondence with the few aneurysms that have been studied microscopically to date.

6.2. THEORETICALLY-MOTIVATED EXPERIMENTS

There are five general steps in the formulation of a constitutive relation (*DEICE*): *D*elineating general characteristics, *E*stablishing a theoretical framework, *I*dentifying a specific form of the relation, *C*alculating best-fit values of the material parameters, and *E*valuating the predictive capability of the final relation. Hsu et al. [42, 43] presented both a new theoretical framework and a multiaxial experimental system for accomplishing steps 2–5 for thin, axisymmetric, non-complicated (i.e., no atherosclerosis and no prior bleeds or repairs) saccular aneurysms. Briefly, the framework exploits two results noted above: equations (14), which show that the in-plane stress-resultants can be determined directly from experimental data, and equation (2), which is a general membrane constitutive relation. Taken together, it is easy to see that, in principle, one can glean information about the response functions $\partial w/\partial E_{\alpha\beta}$ for the material via,

$$\frac{\partial w}{\partial E_{11}} = \frac{\lambda_2}{\lambda_1}\left(\frac{P}{2\kappa_2}\right), \qquad \frac{\partial w}{\partial E_{22}} = \frac{\lambda_1}{\lambda_2}\left(\frac{P}{\kappa_2}\right)\left(1 - \frac{\kappa_1}{2\kappa_2}\right), \tag{15}$$

where $\mathbf{F} = \text{diag}[\lambda_1, \lambda_2]$ and λ_α (stretch ratios), κ_α (principal curvatures), and P (distension pressure) are all experimentally measurable. Although one would prefer to examine these response functions by maintaining one of the principal Green strains constant while the other varies, and vice versa, this is not possible in the axisymmetric inflation problem. Hsu et al. [42] showed via numerical simulations, however, that this approach can provide information on the functional form of the strain-energy function. Unfortunately, this has yet to be accomplished in large part due to the scarcity of unruptured human lesions at autopsy and in particular those having an axisymmetric shape.

6.3. INVERSE FINITE ELEMENT PARAMETER ESTIMATION

Whether the lesion is axisymmetric or non-axisymmetric, or whether the functional form of the strain-energy is identified directly from data or simply postulated, one must calculate best-fit values of the material parameters from data. Kyriacou et al. [59] suggested that the inverse finite element method would be useful in this regard. Briefly, they evaluated this approach by comparing nodal displacements

that were calculated via a (forward) finite element solution (e.g., equations (12)–(13) with an assumed set of material parameters) with those that were found experimentally for an inflated rubber membrane; estimates of the best-fit values of the material parameters were determined by minimizing the difference between computed and measured displacements in a nonlinear least squares sense. Results showed that this approach is indeed feasible, at least for simple material descriptors. Nonetheless, solving the nonlinear finite element equations (iteratively using a Newton–Raphson method) within an iterative nonlinear regression algorithm (Marquardt–Levenberg) can be computationally expensive. Seshaiyer et al. [82] suggested, therefore, that one simply perform the parameter estimation over a subdomain $\Omega_s \subset \Omega_o$, rather than over the whole domain Ω_o. Advantages are two-fold: one avoids the necessity of knowing all of the boundary conditions, which can be challenging even in a laboratory setting, and one need not solve a large number of simultaneous finite element equations.

In particular, Seshaiyer et al. reported best-fit values of the material parameters (constitutive relation similar to equation (1)) based on pressure-strain data from multiple regions from 2 non-axisymmetric human aneurysms. The estimation was based on four linear triangular elements that defined the sub-domain, with the 1 central node "free" and the 4 outer nodes prescribed as displacement boundary conditions. As expected, the results suggested anisotropy and regional differences, the most marked of which was for a lesion that was primarily collagenous but had a region that was visibly atherosclerotic (and thus stiffer). In comparison to the values of the parameters obtained from the data of Scott et al., the more recent findings suggested an overall stiffer behavior. For example, for one (representative) region, $c = 10.18$ N/m, $c_2 = 20.03$, $c_1 = 8.71$, and $c_3 = 8.81$. This was consistent with the much less extensible behavior seen experimentally in these lesions – maximum principal stretches were on the order of 8% rather than the 18% reported by Scott et al. (who assumed that the lesions were perfect spheres). This difference may well have been due to a difference in defining the stress-free states, the more recent data likely being more reliable. Figure 13 shows an illustrative stress–stretch response to equibiaxial stretches of 10% based on the new best-fit values. Note the anisotropy, albeit not marked.

7. Growth and Remodeling

7.1. MOTIVATION

Diverse research over the last 25 years has revealed the ubiquitous role of growth and remodeling within the vasculature, one that is essential to normal tissue maintenance, the process of healing, adaptation to altered conditions, and even the progression or regression of disease. Examples include arterial adaptations to hypertension, sustained alterations in flow, and balloon angioplasty to name but a few [32, 61]. Based on the recent data by Canham and colleagues [66] as well as work on protease activity in aneurysms [31, 69] it appears that stress-mediated

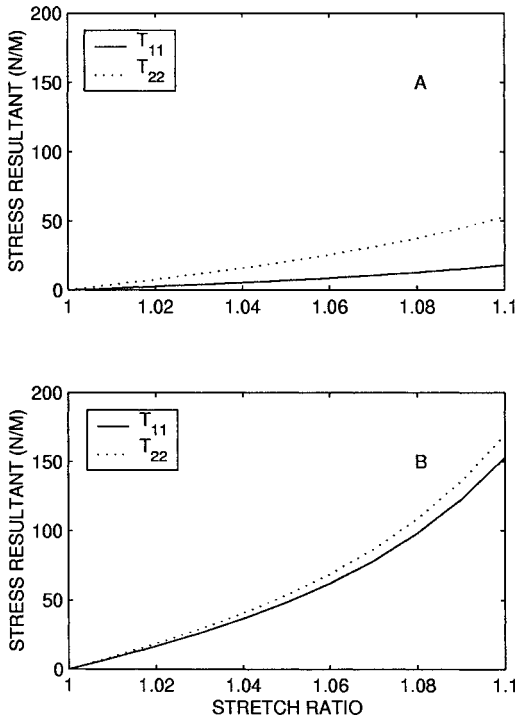

Figure 13. Calculated equibiaxial stress-stretch responses based on the best-fit material parameters determined using the sub-domain inverse finite element method for parameter estimation – results from one region on one human lesion (from Seshaiyer et al., with permission).

regulation of aneurysmal collagen may play a key role in the natural history of these lesions as well. This is largely an open problem from the perspective of mechanics, but let us briefly review recent work that illustrates its potential importance.

7.2. TOWARDS A GROWTH MODEL

There has been only one prior report of a computational model for studying the growth of saccular aneurysms, and unfortunately it is not described in detail. Steiger [95] considered a class of axisymmetric lesions (equations (14)) and stated that "tissue growth rate was set proportional to wall stress". Although there is no discussion of the constitutive or evolution equations, he reports that "sausage-shaped and disc-shaped" lesions tended to develop toward a spherical shape whereas multilobed lesions tended to remain complex. He suggested that localized blebs may be an attempt to stabilize a localized weakness in the wall.

Let us consider the following questions: Can fibroblasts in an enlarging aneurysm synthesize and organize collagen such that the resulting intramural stresses mimic the values experienced in the normal parent vessel? Or, does a particular distribu-

tion of material properties exist that would tend to minimize and homogenize the stress distribution within an aneurysm? In an effort to begin to examine the latter question, Ryan and Humphrey [78] studied 12 sub-classes of non-complicated lesions (maximum dimensions $\leqslant 2$ mm) defined by the triplets (A, B, Z_r) where A and B are the major/minor radii and Z_r is a "truncation level" that yields a model having a neck (cf. Figure 6). Using finite element simulations, preferred material properties were sought in terms of two parameters, $(c_2/c_1)_{\max} \in [1/11, 11]$ and $p \in [1, 6]$, where

$$\frac{c_2}{c_1} = 1 + \left[\left(\frac{c_2}{c_1}\right)_{\max} - 1\right]\left[\frac{i-1}{N-1}\right]^p \tag{16}$$

and c_2 and c_1 are the material parameters in the Fung pseudostrain-energy function (equation (1)), $(c_2/c_1)_{\max}$ is the ratio of these parameters at the neck of the lesion (arc length $S = L$), $i \in [1, N]$ is the finite element number, and p is a descriptor of how (e.g., linearly or nonlinearly) the material symmetry varies from the fundus to the neck. For example, $(c_2/c_1)_{\max} = 1$ implies isotropy at all S, $(c_2/c_1)_{\max} > 1$ yields a progressively increased circumferential stiffness, and $(c_2/c_1)_{\max} < 1$ yields a progressively increased meridional stiffness. Likewise, $p = 1$ requires the symmetry to vary linearly from the fundus to the base (as in Kyriacou and Humphrey [57], Shah et al. [84]), whereas $p > 1$ allows nonlinear variations. Preferred properties thus indicate that particular combination of $(c_2/c_1)_{\max}$ and p that minimizes and homogenizes the stress field.

Based on literally thousands of simulations (though this would be better accomplished simply as an optimization problem), it was found that the multiaxial stresses in lesions having an initially large neck : height ratio tend to be lower and nearly homogeneous if $p > 1$ and $(c_2/c_1)_{\max} > 9$. Figure 14 compares, for example, the different stress distributions for isotropic (i.e., $(c_2/c_1)_{\max} = 1$ and $p = 1$) and the preferred properties for one lesion. With the exception of the boundary layer effect (due to the imposed zero displacement boundary condition at the neck), the stresses are nearly homogeneous. Although results were different for the different geometries (see [78]), the general finding was consistent with that of Steiger [95]): small non-complicated lesions (i.e., thin and collagenous, free of atherosclerosis, fibrin patches, etc.) tended to "prefer" material properties that allowed them to become more spherical. For large neck : height ratios this requires that the lesion expand more in the z direction, which requires less stiffness in the meridional direction; for small neck : height ratios, this requires that the lesion expand more in the r direction, which requires less stiffness in the circumferential direction. These findings are teleologically reasonable as the sphere is the optimal geometry to resist a distension pressure. An unexpected finding, however, was how the lesions preferred to achieve this. For example, lesions with large neck : height ratios tended to concentrate the anisotropy near the neck (i.e., larger values of p).

Although based on idealized models, the finding that intramural stresses in aneurysms can be homogenized simply via a preferential deposition of collagen

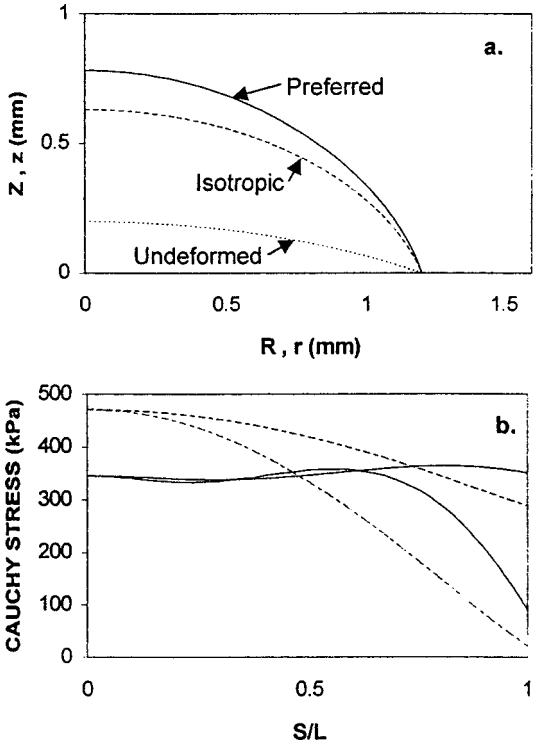

Figure 14. Stress distributions for the same model lesion except that the material behavior is isotropic in one case and "preferred" in the other. Note the tendency towards homogenization and minimization of the stresses in the latter case (from Ryan and Humphrey, with permission).

(and selective removal of old collagen) is provocative. Indeed, given recent reports that apoptosis (programmed cell death) and matrix metalloproteinase activity (matrix degradation) are both increased in saccular aneurysms, and so too for the transcription of type III collagen, it is reasonable to expect significant stress-mediated remodeling in aneurysms [15, 36, 69]. It is tempting to hypothesize, for example, that stable lesions are those which have remodeled in such a way that the stresses experienced by the fibroblasts are restored close to those in the normal parent vessel. There may be cases, of course, wherein the stresses may exceed wall strength prior to the normalization of stress due to remodeling; likewise, the insidious effects of atherosclerosis, the activation of platelets, etc. may also hinder or prevent the remodeling process and thereby lead to rupture. In such cases, the lesion could rupture prior to stabilization. There is clearly a need to explore remodeling theories (e.g., see [48]), which of course must be based on good estimates of the wall shear stress and pressure fields (and thus solid-fluid interactions), which likely serve as signals to the endothelial cells and fibroblasts to control matrix turnover, and better data on the time-course of changes in lesion geometry and microstructure. Only in this way will one be able to formulate and test various

growth and remodeling theories. Much remains to be done, and finite elasticity has a clear role to play.

Acknowledgements

This work was supported in part by grants from the NIH (HL-54957) and the Medical Research Council of Canada. We also wish to acknowledge the expert technical contributions by many individuals in our labs, particularly Helen Finlay, Frank Hsu, Stelios Kyriacou, Donia McDonald, Padhu Seshaiyer, and Amit Shah, as well as our long-standing collaborations with neurosurgery colleagues, Gary Ferguson at the University of Western Ontario and Daniele Rigamonti at the Johns Hopkins Medical Institutions.

References

1. N. Akkas, Aneurysms as a biomechanical instability problem. In: F. Mosora (ed.), *Biomechanical Transport Processes*, Plenum Press (1990) pp. 303–311.
2. G.D. Angelini, S.L. Passani, I.M. Breckenridge and A.C. Newby, Nature and pressure dependence of damage induced by distension of human saphenous vein coronary artery bypass grafts. *Cardiovas. Res.* **21** (1987) 902–907.
3. S. Asari and T. Ohmoto, Growth and rupture of unruptured cerebral aneurysms based on the intraoperative appearance. *Acta Med. Okayama* **48** (1994) 257–262.
4. J.I. Ausman, The New England Journal of Medicine report on unruptured intracranial aneurysms: A critique. *Surg. Neurol.* **51** (1999) 227–229.
5. G.M. Austin, Biomathematical model of aneurysm of the Circle of Willis: The Duffing equation and some approximate solutions. *Math. Biosci.* **11** (1971) 163–172.
6. G.M. Austin, W. Schievink and R. Williams, Controlled pressure-volume factors in the enlargement of intracranial saccular aneurysms. *Neurosurg.* **24** (1989) 722–730.
7. G.M. Austin, S. Fisher, D. Dickson, D. Anderson and S. Richardson, The significance of the extracellular matrix in intracranial aneurysms. *Ann. Clin. Lab. Sci.* **23** (1993) 97–105.
8. M.F. Beatty, Topics in finite elasticity: Hyperelasticity of rubber, elastomers, and biological tissues – with examples. *Appl. Mech. Rev.* **40** (1987) 1699–1734.
9. H.S. Bennett, The microscopical investigation of biological materials with polarized light. In: *McClung's Handbook of Microscopical Technique*, 3rd edn, Hafner Publishing Co., New York (1950).
10. P.J. Camarata, R.E. Latchaw, D.A. Rufenacht and R.C. Heros, State of the art in medicine: Intracranial aneurysms. *Invest. Radiol.* **28** (1993) 373–382.
11. G.J. Campbell and M.R. Roach, Fenestrations in the internal elastic lamina at bifurcations of the human cerebral arteries. *Stroke* **12** (1981) 489–495.
12. P.B. Canham and G.G. Ferguson, A mathematical model for the mechanics of saccular aneurysms *Neurosurg.* **17** (1985) 291–295.
13. P.B. Canham, H.M. Finlay, J.G. Dixon and S.Y. Tong, Aneurysmal fabric modelled by layered great circle trajectories of collagen. *Acta Sterol.* **11** (1992) 703–711.
14. P.B. Canham, H.M. Finlay and S.Y. Tong, Stereological analysis of the layered structure of human intracranial aneurysms. *J. Microsc.* **183** (1996) 170–180.
15. P.B. Canham, H.M. Finlay, J.A. Kiernan and G.G. Ferguson, Layered structure of saccular aneurysms assessed by collagen birefringence. *Neurol. Res.* **21** (1999) 618–626.

16. A.M. Coll, J.F.D. Corral, S. Yazawa and M. Falcon, Intra-aneurysmal pressure differences in human saccular aneurysms. *Neurol.* **6** (1976) 93–96.
17. M.R. Crompton, The pathology of ruptured middle-cerebral aneurysms with special reference to differences between the sexes. *Lancet* **2** (1962) 421–425.
18. M.R. Crompton, Mechanism of growth and rupture in cerebral berry aneurysms. *Br. Med. J.* **1** (1966) 1138–1142.
19. J. Cronin, Biomathematical model of aneurysm of the Circle of Willis: A qualitative analysis of the differential equation of Austin. *Math. Biosci.* **16** (1973) 209–225.
20. S.M. de la Monte, G.W. Moore, M.A. Monk and G.M. Hutchins, Risk factors for development and rupture of intracranial berry aneurysms. *Am. J. Med.* **78** (1985) 957–964.
21. C.J. Doillon, M.G. Dunn, E. Bender and F.H. Silver, Collagen fiber formation in repair tissue: Development of strength and toughness. *Collagen Rel. Res.* **5** (1985) 481–492.
22. J.H. Evans and J.C. Barbenel, Structure and mechanical properties of tendon related to function. *Equine Vet. J.* **7** (1974) 1–8.
23. G.G. Ferguson, Turbulence in human intracranial saccular aneurysms. *J. Neurosurg.* **33** (1970) 485–497.
24. G.G Ferguson, Physical factors in the initiation, growth, and rupture of human intracranial aneurysms. *J. Neurosurg.* **37** (1972) 666–677.
25. G.G. Ferguson, Direct measurement of mean and pulsatile blood pressure at operation in human intracranial saccular aneurysms. *J. Neurosurg.* **36** (1972) 560–563.
26. G.G. Ferguson, Intracranial arterial aneurysms – a surgical perspective. In: *Handbook of Clinical Neurology* 11(55) (1989), pp. 41–87.
27. H.M. Finlay, P. Whittaker and P.B. Canham, Collagen organization in the branching region of human brain arteries. *Stroke* **29** (1998) 1595–1601.
28. W.D. Forbus, On the origin of miliary aneurysms of the superficial cerebral arteries. *Bull. Johns Hopkins Hosp.* **47** (1930) 239–284.
29. G.N. Foutrakis, H. Yonas and R.J. Sclabassi, Finite element methods in the simulation and analysis of intracranial blood flow: Saccular aneurysm formation in curved and bifurcating arteries. Tech Rep 6, Univ of Pitt Comp Neurosci (1994).
30. D.L. Fry, Acute vascular endothelial changes associated with increased blood velocity gradients. *Circ. Res.* **22** (1968) 165–167.
31. P. Gaetani, F. Tartara, F. Tancioni, R. Rodriguez y Baena, E. Casari, M. Alfano and V. Grazioli, Deficiency of total collagen content and of deoxypyridinoline in intracranial aneurysm walls. *FEBS Letters* **404** (1997) 303–306.
32. G.H. Gibbons and V.J. Dzau, The emerging concept of vascular remodeling. *Mech. of Disease* **330**(20) (1994) 1431–1438.
33. Y.P. Gobin, J.L. Counord, P. Flaud and J. Duffaux, In vitro study of hemodynamics in a giant saccular aneurysm model: Influence of flow dynamics in the parent vessel and effects of coil embolization. *Interven. NeuroRadiol.* **36** (1994) 530–536.
34. G.J. Hademenos, T. Massoud, D.J. Valentino, G. Duckwiler and F. Vinuela, A nonlinear mathematical model for the development and rupture of intracranial saccular aneurysms. *Neurol. Res.* **16** (1994) 376–384.
35. G.J. Hademenos, T.F. Massoud, F. Turjman and J.W. Sayre, Anatomical and morphological factors correlating with rupture of intracranial aneurysms in patients referred for endovascular treatment. *Neuroradiol.* **40** (1998) 755–760.
36. A. Hara, N. Yoshimi and H. Mori, Evidence for apoptosis in human intracranial aneurysms. *Neurol. Res.* **20** (1998) 127–130.
37. T. Hasimoto, Dynamic measurement of pressure and flow velocities in glass and silastic model berry aneurysms. *Neurol. Res.* **6** (1984) 22–28.
38. N. Hashimoto and H. Handa, The size of cerebral aneurysms in relation to repeated rupture. *Surg. Neurol.* **19** (1983) 107–111.

39. O. Hassler, Morphological studies on the large cerebral arteries, with reference to the aetiology of subarachnoid haemorrhage. *Acta Psychiatr. Neurol. Scand. (suppl)* **154** (1961) 1–145.
40. O. Hassler, The windows of the internal elastic lamella of the cerebral arteries. *Virchows Arch. Path. Anat.* **335** (1962) 127–132.
41. K. Hegedus, Some observations on reticular fibers in the media of the major cerebral arteries. *Surg. Neurol.* **22** (1984) 301–307.
42. F.P.K. Hsu, C. Schwab, D. Rigamonti and J.D. Humphrey, Identification of response functions for nonlinear membranes via axisymmetric inflation tests: Implications for biomechanics. *Int. J. Sol. Struct.* **31** (1994) 3375–3386.
43. F.P.K. Hsu, A.M.C. Liu, J. Downs, D. Rigamonti and J.D. Humphrey, A triplane video-based experimental system for studying axisymmetrically inflated biomembranes, *IEEE Trans. Biomed. Engr.* **42** (1995) 442–450.
44. J.D. Humphrey, R.K. Strumpf and F.C.P. Yin, A constitutive theory for biomembranes: Application to epicardium. *ASME J. Biomech. Engr.* **114** (1992) 461–466.
45. J.D. Humphrey, Arterial wall mechanics: Review and directions. *Crit. Rev. Biomed. Engr.* **23**(1/2) (1995) 1–162.
46. J.D. Humphrey and S.K. Kyriacou, The use of Laplace's equation in aneurysm mechanics. *Neurol. Res.* **18** (1996) 204–208.
47. J.D. Humphrey, Computer methods in membrane biomechanics. *Comp. Meth. Biomech. Biomed. Engr.* **1** (1998) 171–210.
48. J.D. Humphrey, Remodeling of a collagenous tissue at fixed lengths. *ASME J. Biomech. Engr.* **121** (1999) 591–597.
49. E.J.N. Hung and M.R. Botwin, Mechanics of rupture of cerebral saccular aneurysms. *J. Biomech.* **8** (1975) 385–392.
50. K.K. Jain, Mechanism of rupture of intracranial saccular aneurysms. *Surg*. (1963) 347–350.
51. H. Kamitani, H. Masuzawa, I. Kanazawa and T. Kubo, Bleeding risk in unruptured and residual cerebral aneurysms – angiographic annual growth rate in nineteen patients. *Acta Neurochir. (Wein)* **141** (1999) 153–159.
52. N.F . Kassel and J.C. Torner, Size of intracranial aneurysms. *Neurosurg.* **12** (1983) 291–297.
53. C. Kim, J. Cervos-Navarro, H. Kikuchi, N. Hashimoto and F. Hazama, Alterations in cerebral vessels in experimental animals and their possible relationship to the development of aneurysms. *Surg. Neurol.* **38** (1992) 331–337.
54. M. Kojima, H. Handa, N. Hashimoto, C. Kim and F. Hazima, Early changes of experimentally induced cerebral aneurysms in rats: Scanning electron microscopy study. *Stroke* **17** (1986) 835–841.
55. T.M. Kosierkiewicz, S.M. Factor and D.W. Dickson, Immunocytochemical studies of atherosclerotic lesions of cerebral berry aneurysms. *J. Neuropath. Exp. Neurol.* **53** (1994) 399–406.
56. H. Kraus, *Thin Elastic Shells*, J. Wiley, New York (1967).
57. S.K. Kyriacou and J.D. Humphrey, Influence of size, shape and properties on the mechanics of axisymmetric saccular aneurysms. *J. Biomech.* **29** (1996) 1015–1022. Erratum **30** (1997) 761.
58. S.K. Kyriacou, C. Schwab and J.D. Humphrey, Finite element analysis of nonlinear orthotropic hyperelastic membranes. *Comp. Mech.* **18** (1996) 269–278.
59. S.K. Kyriacou, A. Shah and J.D. Humphrey, Inverse finite element characterization of nonlinear hyperelastic membranes. *J. Appl. Mech.* **64** (1997) 257–262.
60. E.R. Lang and M. Kidd, Electron microscopy of human cerebral aneurysms. *J. Neurosurg.* **22** (1965) 554–562.
61. B.L. Langille, Remodeling of developing and mature arteries: Endothelium, smooth muscle, and matrix. *J. Cardiovasc. Pharmacol.* **21** (1993) S11–S17.
62. Y. Lanir, Constitutive equations for fibrous connective tissues. *J. Biomechanics* **16** (1983) 1–12.

63. J.M. Lee and D.R. Boughner, Tissue mechanics of canine pericardium in different test environments. Evidence for time-dependent accommodation, absence of placticity, and new roles for collagen and elastin. *Circ. Res.* **49** (1981) 533–544.
64. K.O. Lim and D.R. Boughner, Low frequency dynamic viscoelastic properties of human mitral valve tissue. *Cardiovasc. Res.* **10** (1976) 459–465.
65. M. Low, K. Perktold and R. Raunig, Hemodynamics in rigid and distensible saccular aneurysms: A numerical study of pulsatile flow characteristics. *Biorheol.* **30** (1993) 287–298.
66. D.J. MacDonald, H.M. Finlay and P.B. Canham, Directional wall strength in saccular brain aneurysms from polarized light microscopy. *Ann. Biomed. Eng.* **28** (2000) 533–542.
67. F.B. Meyer, J. Huston and S.S. Riederer, Pulsatile increases in aneurysm size determined by cine phase-contrast MR angiography. *J. Neurosurg.* **78** (1993) 879–883.
68. W.R. Milnor, *Hemodynamics*, Williams and Wilkens, Baltimore (1989).
69. C. Mimata, M. Kitaoka, S. Nagahiro, K. Iyama, H. Hori, H. Yoshioka and Y. Ushio, Differential distribution and expressions of collagens in the cerebral aneurysmal wall. *Acta Neuropathol.* **94** (1997) 197–206.
70. G. Neil-Dwyer, J.R. Bartlett, A.C. Nicholls, P. Narcisi and F.M. Pope, Collagen deficiency and ruptured cerebral aneurysms. *J. Neurosurg.* **59** (1983) 16–20.
71. D.A. Nichols, F.B. Meyer, D.G. Piepgras and P.L. Smith, Endovascular treatment of intracranial aneurysms. *Mayo Clinic Proceedings* **69** (1994) 272–285.
72. S.H.M. Nyström, Development of intracranial aneurysms as revealed by electron microscopy. *J. Neurosurg.* **20** (1963) 329–337.
73. J.R. Ostergaard, Risk factors in intracranial saccular aneurysms. *Acta. Neurol. Scand.* **80** (1989) 81–98.
74. J.R. Ostergaard, E. Reske-Nielsen and H. Oxlund, Histological and morphometric observations on the reticular fibers in the arterial beds of patients with ruptured intracranial saccular aneurysms. *Neurosurg.* **20** (1987) 554–558.
75. L. Parlea, R. Fahrig, D.W. Holdsworth and S.P. Lownie, An analysis of the geometry of saccular intracranial aneurysms. *Am. J. Neuroradiol.* **20** (1999) 1079–1089.
76. W.R. Phillips, *Mineral Optics: Principles and Techniques,* W.H. Freeman, San Francisco (1971), pp. 171–190.
77. C. Richardson and O. Kofman, Cranial bruit with intracranial saccular aneurysms. *Trans. Am. Neurol. Assoc.* **76** (1951) 151–154.
78. J.M. Ryan and J.D. Humphrey, Finite element based predictions of preferred material symmetries in saccular aneurysms. *Ann. Biomed. Engr.* **27** (1999) 641–647.
79. A.L. Sahs, Observations on the pathology of saccular aneurysms. *J. Neurosurg.* **24** (1966) 792–806.
80. L.N. Sekhar and R.C. Heros, Origin, growth and rupture of saccular aneurysms: A review. *Neurosurg.* **8** (1981) 248–260.
81. L.N. Sekhar, R.P. Sclabassi, M. Sun, H.B. Blue and J.F. Wasserman, Intra-aneurysmal pressure measurements in experimental saccular aneurysms in dogs. *Stroke* **19** (1988) 353–356.
82. P. Seshaiyer, A.D. Shah, S.K. Kyriacou and J.D. Humphrey, Multiaxial mechanical behavior of human saccular aneurysms. *Comp. Meth. Biomech. Biomed. Engr.* **4** (2001) 281–290.
83. S. Scott, G.G. Ferguson and M.R. Roach, Comparison of the elastic properties of human intracranial arteries and aneurysms. *Can. J. Physiol. and Pharmacol.* **50** (1972) 328–332.
84. A.D. Shah, J.L. Harris, S.K. Kyriacou and J.D. Humphrey, Further roles of geometry and properties in saccular aneurysm mechanics. *Comp. Meth. Biomech. Biomed. Engr.* **1** (1997) 109–121.
85. A.D. Shah and J.D. Humphrey, Finite strain elastodynamics of saccular aneurysms. *J. Biomech.* **32** (1999) 593–599.
86. T.E. Simkins and W.E. Stehbens, Vibrational behavior of arterial aneurysms. *Lett. Appl. Engr. Sci.* **1** (1973) 85–100.

87. J.H.F. Smith, P.B. Canham and J. Starkey, Orientation of collagen in the tunica adventitia of the human cerebral artery measured with polarized light and the universal stage. *J. Ultrastruct. Res.* **77** (1981) 133–145.
88. J. Starkey, The analysis of three-dimensional orientation data. *Can. J. Earth Sci.* **30** (1993) 1355–1362.
89. W.E. Stehbens, Histopathology of cerebral aneurysms. *Arch. Neurol.* **8** (1963) 272–285.
90. W.E. Stehbens, Ultrastructure of aneurysms. *Arch. Neurol.* **32** (1975) 798–807.
91. W.E. Stehbens, The pathology of intracranial arterial aneurysms and their complications. In: J.L. Fox (ed.), *Intracranial Aneurysms*, Springer-Verlag, New York (1983).
92. W.E. Stehbens, Pathology and pathogenesis of intracranial berry aneurysms. *Neurol. Res.* **12** (1990) 29–34.
93. H.J. Steiger, R. Aaslid, S. Keller and H.J. Reulen, Strength, elasticity and viscoelastic properties of cerebral aneurysms. *Heart Vessels* **5** (1986) 41–46.
94. H.J. Steiger, D.W. Liepsch, A. Poll and H.J. Reulen, Hemodynamic stress in terminal saccular aneurysms: A laser doppler study. *Heart Vessels* **4** (1988) 162–169.
95. H.J. Steiger, Pathophysiology of development and rupture of cerebral aneurysms. *Acta Neurochir. Suppl.* **48** (1990) 1–57.
96. J. Suzuki and H. Ohara, Clinicopathological study of cerebral aneurysms. *J. Neurosurg.* **48** (1978) 505–514.
97. M. Toth, G.L. Nadasy, I. Nyary, T. Kerenyi, M. Orosz, G. Molnarka and E. Monos, Sterically inhomogeneous viscoelastic behavior of human saccular cerebral aneurysms. *J. Vasc. Res.* **35** (1998) 345–355.
98. H. Ujiie, K. Sato, H. Onda, A. Oikkawa, M. Kagawa, K. Atakakura and N. Kobayashi, Clinical analysis of incidentally discovered unruptured aneurysms. *Stroke* **24** (1993) 1850–1856.
99. H. Ujiie et al., Effects of size and shape (aspect ratio) on the hemodynamics of saccular aneurysms: A possible index for surgical treatment of intracranial aneurysms. *Neurosurg.* **45** (1999) 119–130.
100. R. Vilarta and B.C. Vidal, Anisotropic and biomechanical properties of tendons modified by exercise and denervation: Aggregation and macromolecular order in collagen bundles. *Matrix* **9** (1989) 55–61.
101. S.A. Wainwright, W.D. Biggs, J.D. Currey and J.M. Gosline, *Mechanical Design in Organisms*, Princeton University Press (1976), pp. 88–93.
102. D.O. Wiebers, J.P. Whisnant, T.M. Sundt and W.M. O'Fallon, The significance of unruptured intracranial aneurysms. *J. Neurosurg.* **66** (1987) 23–29.
103. D.O. Wiebers et al., Unruptured in tracranial aneurysms – risk of rupture and risks of surgical intervention. International study of unruptured intracranial aneurysms investigators. *N. Engl. J. Med.* **339** (1998) 1725–1733.
104. P. Whittaker, M.E. Schwab and P.B. Canham, The molecular organization of collagen in saccular aneurysms assessed by polarized light microscopy. *Conn. Tiss. Res.* **17** (1988) 43–54.
105. P. Whittaker, D.R. Boughner and R.A. Kloner, Role of collagen in acute myocardial infarct expansion. *Circulation* **84** (1991) 3123–3134.
106. M. Wolman and T.A. Gillman, A polarized light study of collagen in dermal wound healing. *Br. J. Exp. Path.* **53** (1972) 85–89.